



HAL
open science

77GHz ACC radar simulation platform

Camilla Kärnfelt, Alain Peden, Ali Bazzi, Ghayath El Haj Shhade, Mohamad Abbas, Thierry Chonavel, Frantz Bodereau

► **To cite this version:**

Camilla Kärnfelt, Alain Peden, Ali Bazzi, Ghayath El Haj Shhade, Mohamad Abbas, et al.. 77GHz ACC radar simulation platform. ITST 2009 : 9th international conference on Telecommunications for Intelligent Transport Systems, Oct 2009, Lille, France. 10.1109/ITST.2009.5399354 . hal-00446338

HAL Id: hal-00446338

<https://hal.science/hal-00446338>

Submitted on 3 Jun 2024

HAL is a multi-disciplinary open access archive for the deposit and dissemination of scientific research documents, whether they are published or not. The documents may come from teaching and research institutions in France or abroad, or from public or private research centers.

L'archive ouverte pluridisciplinaire **HAL**, est destinée au dépôt et à la diffusion de documents scientifiques de niveau recherche, publiés ou non, émanant des établissements d'enseignement et de recherche français ou étrangers, des laboratoires publics ou privés.

77 GHz ACC Radar Simulation Platform

Camilla Kärnfelt, Alain Péden, Ali Bazzi, Ghayath El Haj Shhadé, Mohamad Abbas,
Thierry Chonavel and Frantz Bodereau

Abstract—The development of a system simulation platform for Adaptive Cruise Control (ACC) radar working at 77 GHz is presented. The simulation platform allows us to test different radar architectures, modulation formats and detection algorithms as well as to simulate different scenarios, which improves the decision-making before and during the hardware development.

Index Terms—Automotive Radar, Adaptive Cruise Control, Modulation Format, LFM, FMCW

I. INTRODUCTION

TO improve and add functionality to ACC radars, a system simulator that takes into account the radar's front-end performance at 77 GHz as well as the signal modulation and signal processing at base-band frequencies, is a must. We presented such a radar simulation platform for Frequency Shift Keying (FSK) modulation format in 2007, [1]. Generally FSK based radars have excellent speed resolution, but the distance resolution is not very good. This makes it difficult to discriminate between two targets with identical relative speed, and further, targets with the same speed as the radar, i.e. a zero relative speed, are not detected at all. This is why a Linear Frequency Modulation (LFM) format that allows the handling of more complex scenarios, [2], has been chosen as the modulation format for our work, and a second-generation simulation platform using LFM was recently presented in [3].

This paper reports on some improvements of the latter of these simulation platforms: noise has been introduced in the front-end components, new modulation formats for better beat frequency association at multiple-target-scenarios have been added and finally a MATLAB script has been developed to enhance the signal treatment using target identification algorithms.

II. LFM WAVEFORMS

One basic LFM waveform is the Frequency Modulated Continuous Wave (FMCW), as presented in Fig. 1, see also [4]-[6]. When using this modulation format the target detection is obtained from the beat frequencies presented for each target on the up and down ramp respectively. The beat frequency obtained on the up ramp is denoted by f_{b+} and on the down ramp it is denoted f_{b-} . The two beat frequencies can be calculated according to eq. (1), where v_r is the relative speed of the target, f_0 the carrier frequency, c the speed of light, f_m

the modulation bandwidth, R the range and T_r denotes the total duration of the up and down ramps.

$$f_{b\pm} = \frac{2 \cdot v_r \cdot f_0}{c} \mp \frac{f_m \cdot 4 \cdot R}{T_r \cdot c} \quad (1)$$

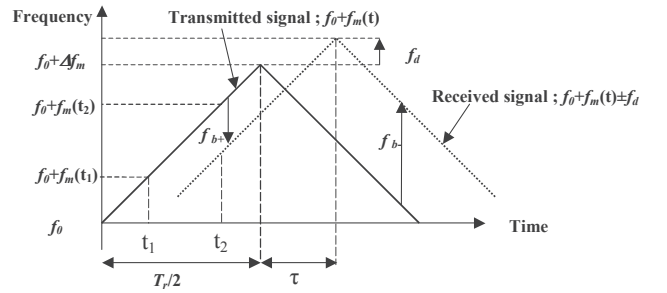


Fig. 1. FMCW modulation waveform.

Once having detected the beat frequencies the related target's data are found by the following manipulations: by adding f_{b+} to f_{b-} and solving for v_r , the relative speed is obtained and by subtracting f_{b-} from f_{b+} and solving for R the range is obtained. This is summarized in the following equations:

$$v_r = \frac{c}{4 \cdot f_0} (f_{b+} + f_{b-}) \quad (2)$$

$$R = -\frac{T_r \cdot c}{8 \cdot f_m} (f_{b+} - f_{b-}) \quad (3)$$

In this paper a double FMCW modulation format (Frequency Modulated Continuous Wave with two up and down ramps) is used. This waveform is inspired by the one proposed in [6].

The two triangles do not have exactly the same size. Thus, there is a small difference of the ramp (or chirp) inclination between the first and the second triangle. This ensures, as was shown in [6], that the sequence order of the targets' beat frequencies remains the same for the up and down ramp respectively. The correct association between the beat frequencies of the different ramps is thus guaranteed, which is otherwise a problem for a single triangle FMCW.

When using this double FMCW modulation format, four beat frequencies are associated with each target, one on each ramp, and the associated equations for calculating the targets relative speed and range are given in eq. (4) and (5). Here f_{b+} denotes the beat frequency on the first up ramp, f_{b-} the one on the first down ramp, f_{b+} the one on the second up ramp and finally f_{b-} the one on the second down ramp. T_r is the total duration of the wave form (5.12 ms) and θ is the duration of

the first triangle (2.695 ms). The carrier frequency, f_0 , used is 76.5 GHz and the modulation bandwidth, f_m , is 600 MHz.

$$v_r = \frac{c}{8 \cdot f_0} (f_{b+'} + f_{b-'} + f_{b+''} + f_{b-''}) \quad (4)$$

$$R = -\frac{c((f_{b+'} - f_{b-'}) + (f_{b+''} - f_{b-''}))}{8 \cdot f_m \cdot \left(\frac{1}{\theta} + \frac{1}{T_r - \theta} \right)} \quad (5)$$

III. THE RADAR SIMULATION PLATFORM

In order to obtain a usable simulation platform, the complete front-end, which consists of the microwave monolithic integrated circuits (MMIC), the propagation channel, the antenna and the targets, has to be modeled correctly, including precise noise characteristics. We have chosen to develop the MMIC models based on vendors' specifications. The other sub-circuits are represented by their scattering parameters found by electromagnetic simulations. The antenna is described by its gain, and the propagation channel by a time delay and attenuation related to the distance. Four types of targets, differentiated by their Radar Cross Section (RCS), are modeled (pedestrian, motorcycle, car, truck).

The radar architecture is shown in Fig. 2. The yellow boxes indicate the parameters on transmission and the violet boxes the reception. The I and Q data yield the sign of the beat frequency and thereby the targets' relative speed.

The Radar platform is developed in the Advanced Design System software from Agilent, with its built-in Envelope simulator and base-band Data Flow controller that handle the flow of the digital signal processing. The Envelope simulator is launched from the Data Flow controller that also applies the modulation to the Voltage Controlled Oscillator (VCO) and collects the base-band data.

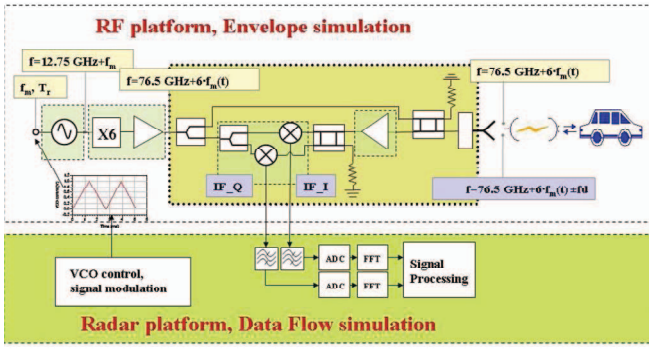


Fig. 2. The general radar architecture and simulation platform, where the Data Flow simulation tool controls the Envelope simulation of the RF platform.

Table 1 presents the device data used in this simulation platform.

A. MMIC modeling

The complete set of MMICs intended to be used in this radar are commercially available from the UMS foundry. The related specifications are found in [7]-[10].

TABLE 1. DATA OF THE RADAR FRONT-END COMPONENTS

Component	Parameter	Value	
VCO (MMIC)	Frequency	12.75 GHz + f_m	
	Output power	5 dBm	
	Phase Noise at 10kHz	-75 dBc/Hz	
	at 100 kHz	-100 dBc/Hz	
	at 1 MHz	-123 dBc/Hz	
Multiplier-by-six-amplifier (MMIC)	Multiplication factor	6	
	Output power	14.5 dBm	
	Noise figure	8 dB	
Low Noise Amplifier (MMIC)	Gain	15 dB	
	Noise figure	4.5 dB	
Mixer (MMIC)	Conversion loss	7.5 dB	
	Noise figure at 1kHz	34 dB	
	at 10 kHz	28 dB	
	at 100 kHz	21 dB	
	at 200 kHz	17 dB	
Couplers (Duroid)	Losses	3.2 dB	
	Isolation	40 dB	
Transition (antenna)	Losses	0.25 dB	
Antenna	Maximal gain (TX)	27 dB	
	Surface effective area (RX)	$6.06 \cdot 10^{-4} \text{ m}^2$	
	Noise temperature	$\sim 290 \text{ K}$	
Propagation path	Losses (per unit area)	$10 \log_{10}(4\pi R^2) \text{ dBsm}$	
	Delay	$\tau = R/c \text{ s}$	
Targets	Doppler frequency	$2v_r f_0 / c \text{ Hz}$	
	RCS	Pedestrian	-10 dBsm
		Motorcycle	7 dBsm
	Car	min	$10 \log_{10}(R) + 5 \text{ dBsm}$
			20 dBsm
Truck	min	$20 \log_{10}(R) + 5 \text{ dBsm}$	
		45 dBsm	

1) Voltage Control Oscillator (VCO)

The VCO, [7], is modeled by a VCO block and a phase noise modulator block. The oscillation frequency is set to 12.75 GHz, the output power is set to 5 dBm (14 dBm is also possible but not necessary since the following MMIC circuit includes a Medium Power Amplifier), and the tuning frequency is set to 100 MHz/V. The parameters in the phase noise block are chosen as to result in a phase noise that is as close as possible to the values listed in the specification, see Table 1. The resulting phase noise curve is presented in Fig. 3.

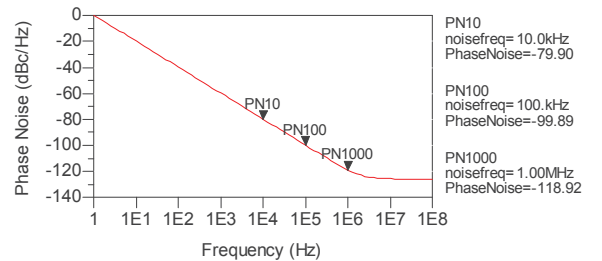


Fig. 3 The VCO phase noise (dBc/Hz) as a function of frequency (Hz).

2) Multiplier by Six-Medium Power Amplifier (X6MPA)

The X6MPA, [8], is modeled by a frequency multiplying block, an amplifier block and a noise voltage source connected to an AM modulator.

In the multiplying block, the gain of the unwanted harmonics is set to -60 dB and the gain of the wanted 6th harmonic is set to 0 dB.

In the amplifier block the forward transmission coefficient (or gain) is set to 9 dB (which will result in a 14 dBm output power). The gain compression parameters are adjusted to achieve an output power versus input power plot after harmonic balance simulations as depicted in Fig. 4.

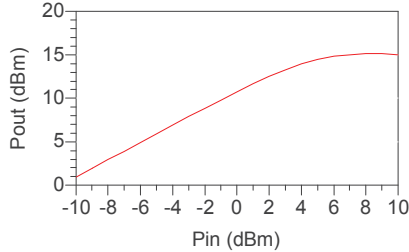


Fig. 4. The MPA power gain obtained after the harmonic balance simulation.

The phase noise increase, caused by the frequency multiplier, can be calculated as $20 \cdot \log_{10}(N)$ where N is the multiplication factor. Thus the increase due to the multiplier by six is 15.6 dB which is seen when comparing the phase noise of the output of the VCO with that of the output of the multiplier block, see Fig. 5.

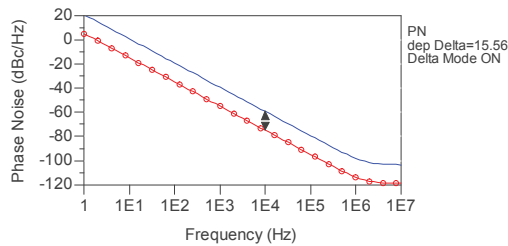


Fig. 5. The phase noise due to the multiplier by six after simulation follows the theoretically calculated value, as expected. VCO phase noise (o), phase noise after the multiplier by six (-).

As an amplifier has a multiplication factor of 1 (i.e. only the fundamental signal and no harmonics on the output) the phase noise increase due to the MPA should be $20 \cdot \log_{10}(1)=0$ and as a result the phase noise difference from the VCO output to the MPA output should be 15.6 dB. However, plotting the phase noise at the output of the MPA and again comparing this value to the phase noise at the VCO output, we see that here the difference is only 12.6 dB, which should indicate that the MPA has actually decreased the phase noise in the circuit.

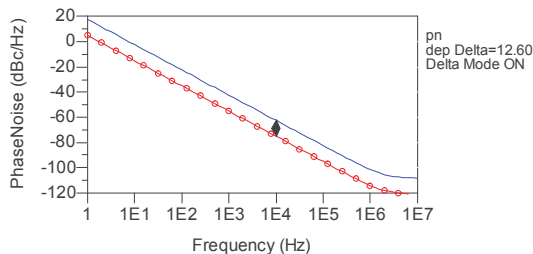


Fig. 6. The phase noise at the output of the MPA as compared to the output of the VCO. The difference is less than the theoretically calculated value and is due to the MPA saturation. VCO phase noise (o), phase noise after the X6MPA (-).

This phenomenon which occurs in the amplifiers' saturated

region is described and explained in [11]. In the radar front-end application, the MPA works in the saturated region.

3) Low Noise Amplifier (LNA)

The LNA, [9], is modeled with an amplifier block with the forward transmission coefficient set to 15 dB and the noise figure set to 4.5 dB. The gain compression parameters were adjusted for the power gain plot to fit the specification, see Fig. 7.

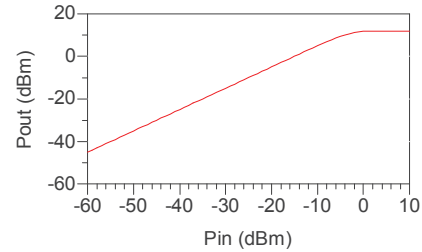


Fig. 7. The LNA output power versus input power.

4) Mixer

The mixer used is a dual channel mixer, [10], with a typical conversion loss of 7.5 dB at the system frequency. The low frequency noise figure of this component varies with the frequency due to the $1/f$ noise generation, see Table 1.

The mixer is modeled by a mixer block with the noise figure set to 17 dB and the conversion gain to -7.5 dB. The $1/f$ noise is then generated in a noise voltage source block and then added to the output signal. In fact, the noise voltage parameter is given by an equation ($V_{Noise}=k/(min_IFfrequency)^b$) with k and b adjusted to obtain the correct $1/f$ noise profile. It was found that k should be $6 \cdot 10^{-7}$ and $b=0.45$ for the best fit. The parameter $min_IFfrequency$ is chosen as the lowest down converted beat frequency for each ramp according to the targets' distances and relative speeds, which thus sets the associated noise for that ramp. This means that the noise level is not the same on the four ramps and the signal to noise ratio (SNR) has to be monitored on each ramp separately.

Since there is no sensor block within ADS that can be used to, within the mixer model during simulation, determine which is the lowest down converted frequency, the model has to be provided with this information. Thus, for each simulation case, a set of case specific distance/relative speed data is given as input parameters to the ADS model. From these parameters, the minimum beat frequency on each ramp is calculated (using Variable Equations within the ADS model) and used as the $min_IFfrequency$ to provide the ramp and case specific $1/f$ noise.

B. Modeling of passive elements

1) Passive elements on the mm-wave card

The passive elements on the mm-wave card are modeled in two ways; one using the ADS provided microstrip blocks such as power splitter for the power divider placed after the X6MPA output, a 4-port S-parameter block with ideal coefficients for the circulator (which is in fact realized as a 3 dB/90° dB hybrid). In this version no transmission lines are

used since they do not add any functionality to the platform evaluation.

In the second version the whole mm-wave card is modeled using the ADS Momentum simulator tool, and thus a “look-alike” circuit is introduced in the platform. The difficulty with this more realistic approach is that the Momentum card model has to be optimized to provide an excellent LO isolation in order to avoid the generation of a large DC signal on the mixer output. In reality a DC component in the output spectrum is probable, however this is eliminated in the filter before the Fourier transformation takes place and it could therefore be omitted from. The 3 dB/90° hybrid Momentum simulation data are presented in Fig. 8.

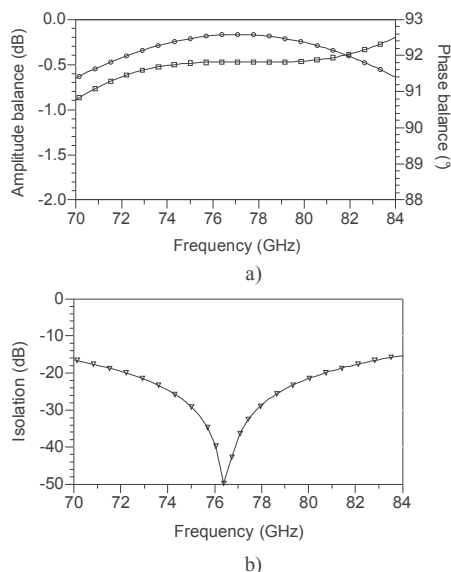


Fig. 8. The momentum simulation results for the coupler circuit on 127 μm thick, Rogers RT 5880, Duroid: a) Amplitude (o) and phase balance (□) versus frequency, b) Isolation versus frequency.

2) Microwave line to waveguide transition

To interconnect the mm-wave card to the antenna a microstrip to waveguide transition is used. This transition is modeled using the Ansoft HFSS electromagnetic simulator tool, see Fig. 9. The microstrip line ends in a patch probe which excites a wave guide of WR10 size. A metal short circuit is placed at a distance of $\lambda_g/4$ over the patch probe, which will serve as an open circuit in the feed plane enabling maximum electrical field strength.

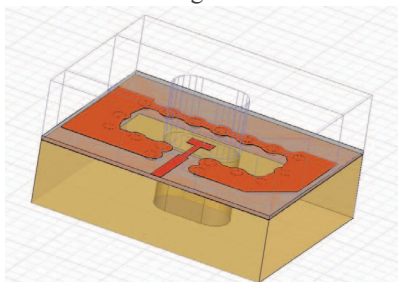


Fig. 9. HFSS model of the microstrip to waveguide transition.

The forward transmission loss of this transition is 0.24 dB at the carrier frequency and better than 0.5 dB from 70 to

90 GHz. The reflection coefficients are better than -12 dB from 70 to 90 GHz with a minimum of -23 dB at the design frequency.

3) Antenna

The antenna is subject to detailed investigation throughout this project, since the choice of antenna concept has a great impact on the overall cost of the radar system. However, since the antenna development has been running in parallel with the simulation platform work, a simple antenna model has been used until the final choice is made and the actual antenna gain and radiation pattern can be entered in the platform simulator.

The antenna is designed for a narrow lobe width which is swept over the road, thus the target’s angular position is given by the sweep angle. This time dependent sweep behavior is not taken in concern in the simulation platform, but a forward pointing antenna is modeled by an output and an input amplifier block. The output amplifier has a forward transmission coefficient set to 27 dB whereas for the input amplifier it is calculated by the effective area as $G_R \lambda^2 / (4 \cdot \pi)$. Here G_R denotes the reception gain which is 27 dB, and λ is the free space wavelength at the carrier frequency.

4) Propagation channel

The propagation channel is represented by an attenuator block and a time delay block in each direction (i.e. transmission and reflection mode). For simplicity, only the Line of Sight (LOS) propagation path is considered, since the road reflected propagation path delivers a much weaker reflected signal which is shifted in frequency less than the frequency resolution of the simulation platform permits to detect. Moreover, the fact that some targets might be concealed by the others is not taken into account.

5) Targets

Four targets are used in this study: the pedestrian, the motorcycle, the car and the truck. The model parameters are the radar cross section (RCS) and the Doppler frequency shift associated to target’s relative speed. A few papers presenting results from measurements of the radar cross section at 76 GHz exist, e.g. [12]-[16].

In [12], measurements are performed from 50 to 94 GHz for several test vehicles in each group: motorcycles, cars and minivans, while varying the direction of the vehicles from -10° to $+10^\circ$ azimuth. These results show a clear difference in the RCS depending on the frequency and azimuth. In [14] the RCS for a pedestrian at 76 GHz and a 5 m distance is found to be -8 dBsm. However, it is noted that this value varies a lot depending on the clothing of the pedestrian. In [15] the variation of the RCS of a car at 76 GHz is measured for two distances, 5 m and 25 m, and found to be about 2 and 16 dBsm respectively. This shows that the RCS for large targets varies with distance in the near field range. Consequently, a fix RCS value can only be used at a distance sufficiently large for the whole target to be illuminated by the lobe. When the target is close to the radar, the radar lobe only illuminates a smaller part of the vehicle and therefore the RCS must be varied

accordingly.

Other results extracted from ray tracing simulations and measurement validations have also been proposed in [16] where an azimuth dependent RCS is achieved.

Hence, from all this, we can conclude that the RCS for different targets depend on the frequency, azimuth angle, distance, etc., and to be able to model the radar's behavior a set of RCS for the targets must be found. In this work, the two smaller targets are modeled with a fix RCS value: -10dBsm and 7dBsm for the pedestrian and the motorcycle respectively. For the two larger targets, a modeling approach, taking into account the RCS dependence of the distance, while fixing the carrier frequency at 76.5 GHz and the azimuth at 0° , has been taken. To find an empirical formula to model the car's and truck's RCS, we have performed measurements using an antenna with a 5° lobe angle, an azimuth angle to the target of 0° and the distance, R , was then varied. The formulas obtained are presented in equation (6) and (7) below:

$$RCS_{car} = \min \left\{ \begin{array}{l} 10 \cdot \log_{10}(R) + 5 \\ 20 \end{array} \right. \quad (\text{dBsm}) \quad (6)$$

$$RCS_{truck} = \min \left\{ \begin{array}{l} 20 \cdot \log_{10}(R) + 5 \\ 45 \end{array} \right. \quad (\text{dBsm}) \quad (7)$$

The RCS for the four targets are represented in Fig. 10 below. Also included are the referenced RCS values, [12]-[15], given at 76 GHz for comparison. The values deviate from each others, probably because of the angular beam width of the antenna not given in these references.

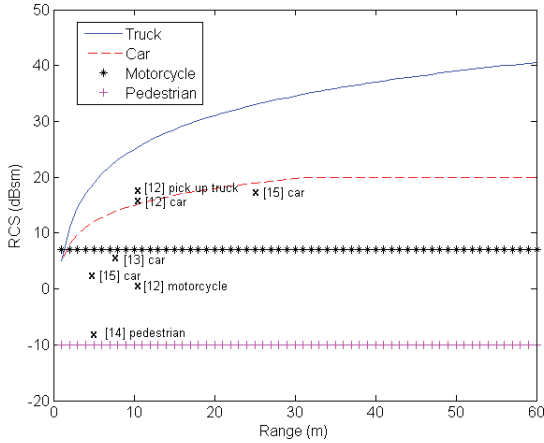


Fig. 10. Radar cross section used throughout the simulations: car according to eq. (6), truck according to eq. (7), motorcycle 7 dBsm and pedestrian -10 dBsm . Other published data, [12]-[15].

IV. SIMULATION EXAMPLE

Fig. 11. a shows the double FMCW modulation wave form used in the following simulation example where the targets are a truck [15 m, $+80\text{ km/h}$, $RCS=28.5\text{ dBsm}$], a pedestrian [15 m, $+10\text{ km/h}$, $RCS=-10\text{ dBsm}$], and a motorcycle [150m, $+10\text{ km/h}$, $RCS=7\text{ dBsm}$]. Fig. 11.b shows the acquired down-converted signal from this simulation.

Since we have three targets and consequently three beat frequencies on each ramp, we should expect to detect the sum

of these three beat frequencies in Fig. 11. b, while we seem to observe only a pure sinusoid wave. This is due to the fact that, for this specific simulation case, there is a very strong power difference between the three reflected signals. The time observation only reveals the beat frequency of the most powerful reflected signal (which comes from the truck at 15 m). Nevertheless, all beat frequencies with a power greater than the noise level will be detected by means of Fourier analysis.

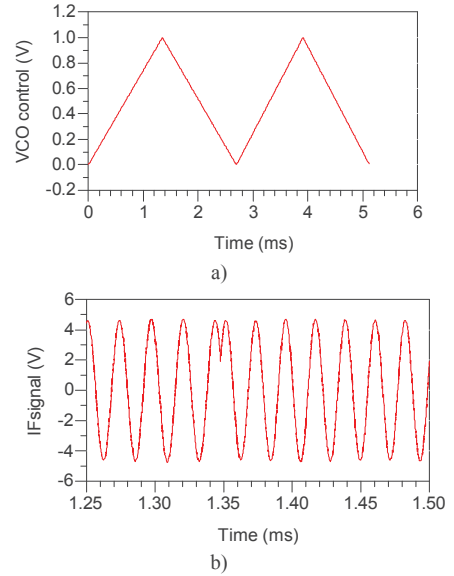


Fig. 11. a) Double FMCW modulation format. b) The returned down-converted signal's I component, for the simulation example, around the first maximum modulation frequency.

A. Signal Processing

Once the IF I and Q signals are acquired, the signal processing is to be carried out.

For an appropriate signal processing, several basic functionalities are required:

1. The signal spectrum for each ramp has to be calculated.
2. All peaks in the spectrum above a given noise level have to be detected and saved in a table. Here a target that returns a beat frequency with an SNR above 15 dB is considered as detectable.
3. False targets have to be eliminated and the remaining peaks in each spectrum have to be associated correctly.
4. Once the association is done, the sign of each beat frequency has to be determined for correct distance and relative speed calculation.
5. The targets' types can then be classified from their estimated RCS.

1) Signal processing in ADS

In ADS, built-in spectrum analyzers are used to capture the frequency spectrum of each ramp, as shown in Fig. 12. Unfortunately, once the spectra are available, the ADS data display offers very limited possibilities to automatically detect the peaks that reach above the noise floor and there is no loop function available (which is a must for the association of peaks). Hence, the peak-detection-association and target-

identification algorithm is almost impossible to implement. Therefore, the time-variant base-band components (I and Q) of the received signal (as in Fig. 11.b) are exported for further processing in MATLAB.

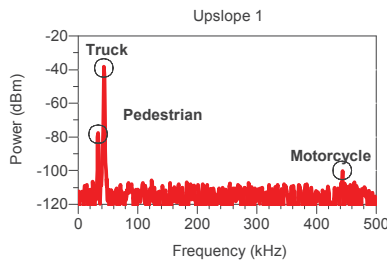


Fig. 12. Frequency spectrum of the first up ramp of the simulation example, from the ADS data display.

2) Improved Signal Processing using MATLAB

Using MATLAB we perform the following operations to obtain the target information from the ADS radar simulation:

1. The imported I and Q components are combined to a complex signal, which is then divided into pieces, with lengths equal to the time of each modulation ramp.
2. A Hanning window is applied to reduce fluctuations in the spectra.
3. Fourier transformation with zero-padding is applied to each signal piece to enhance the estimation of the beat frequencies.
4. The power is calculated and spectra are plotted.
5. The noise level of each spectrum is calculated over the actual bandwidth (1/ramp duration).
6. The peaks' locations are achieved by detection thresholding, which yields frequency intervals where they lie. Within these intervals, the local maximum is found and identified as a beat frequency, if the SNR is better than 15 dB.
7. The association of peaks found in the spectra is made by comparison of their sequence order and power. Hence, false alarms (random noise peaks) can be eliminated.
8. The related targets' data are calculated and the targets are classified.

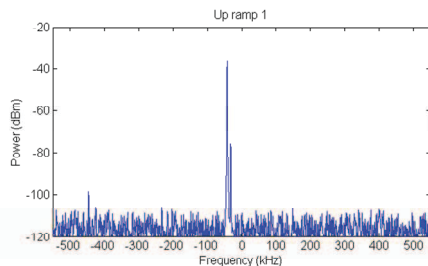


Fig. 13. The spectrum for the first up ramp, obtained using the MATLAB signal processing.

In Fig. 13 the first up ramp spectrum from the MATLAB signal processing is presented (c.f. the corresponding spectra in Fig. 11.b delivered by ADS). Here, the beat frequencies occur to be negative, which is in fact correct as can be verified by entering the targets data in eq. (1), while setting T_r equal to θ , which is the duration of the first triangle. So, using the

complex signal in the FFT, we receive directly the correct sign information for the beat frequencies.

Fig. 14 shows that the MATLAB script has found the targets, and their parameters are calculated correctly. The SNR for the three targets are well above the detection limit of 15 dB, and consequently the three targets are detected.

	Distance	Speed	RCS	SNR	Type
1	150.0661	9.5712	6.7473	30.8653	Motorcycle
2	15.0000	10.9911	28.3325	93.2866	Truck
3	15.0001	79.5228	-10.4540	54.7030	Pedestrian

Fig. 14. Results presented after processing the simulation data with MATLAB for the example in Fig. 11.b. and Fig. 13.

V. CONCLUSIONS

We have developed a full system radar simulator using ADS simulations combined with a MATLAB script for efficient signal processing. Different architectures, modulation formats and detection algorithms can therefore be studied before the hardware is realized.

REFERENCES

- [1] G. Piel, A. Péden, and P. Mallejac, "Virtual platform for the design and the analysis of the performance of an adaptive cruise control radar," *ITST 5th International Conference on ITS Telecommunications*, Brest, France, June 2005.
- [2] H. Rohling, and M.-M. Meinecke "Waveform design principles for automotive radar systems," *CIE International Conference on Radar*, Beijing, China, Oct. 2001.
- [3] C. Kärnfelt, A. Péden, G. El Haj Shhadé, M. Abbas and F. Bodereau, "Plate-forme de simulation globale pour radar ACC à 77 GHz," *CoGIST09*, St Quay Portrieux, France, June 2009, pp. 131-138.
- [4] H. Ruser, and V. Mágori, "Sweep linearization of a microwave FMCW doppler sensor by an ultrasonic reference," *Proceedings of the 1997 IEEE International Frequency Control Symposium*, pp. 201-206.
- [5] M.-M. Meinecke, H. Hermann, "Combination of LFMCW and FSK modulation principles for automotive radar systems," *German Radar Symposium GRS2000*, Berlin, Oct. 11-12, 2000
- [6] S. Miyahara, "New algorithm for multiple object detection in FM-CW radar," *SAE Technical Paper Series 2004-01-0177*.
- [7] www.ums-gaas.com CHV2270 rev 30Jan09 (homepage visited 25 august 2009).
- [8] www.ums-gaas.com CHU3377 rev 23Mar07 (homepage visited the 25 august 2009).
- [9] www.ums-gaas.com CHA1077a rev 21Oct08 (homepage visited the 25 august 2009).
- [10] www.ums-gaas.com CHM2378a rev 20Dec06 (homepage visited the 25 august 2009).
- [11] A. Geens and Y. Rolain, "Noise behavior of an amplifier in compression," *Digest-spring of 55th ARFTG Conference*, Vol. 37, June 2000, pp.1-8.
- [12] H. Suzuki, "Radar cross section of automobiles for millimeter wave band," *JARI research Journal*, Vol. 22, No. 10, pp. 475-478, 2000.
- [13] N. Yamada, "Three-dimensional high resolution measurement of radar cross section for car in 76 GHz band," *R&D review of Toyota Central R&D Labs.*, Vol. 36, No. 2 (2001. 6).
- [14] N. Yamada, "Radar cross section for pedestrian in 76 GHz," *Proceedings of 2005 European Microwave Conference*, Vol. 2, 4-6 Oct. 2004, pp.46-51.
- [15] R. Schneider, H.-L. Blöcher, K. M. Strohm, "KOKON – Automotive high frequency technology at 77/79 GHz," *Proceedings of the 4th European Radar Conference*, October 2007, Munich, Germany, pp. 247-250.
- [16] K. Schuler, D. Becker, and W. Wiesbeck, "Extraction of vertical scattering centers of vehicles by ray-tracing simulations," *IEEE Transactions on Antennas and Propagation*, Vol. 56, No. 11, November 2008, pp. 3543-3551.